Available online at www.sciencedirect.com

SciVerse ScienceDirect

Scripta Materialia 66 (2012) 706–709

Scripta MATERIALIA

www.elsevier.com/locate/scriptamat

Intrinsic size-controlled strain hardening behavior of nanolayered Cu/Zr micropillars

S. Lei,[a,1] J.Y. Zhang,[a,1] J.J. Niu,[a] G. Liu,[a,*] X. Zhang[b,*] and J. Sun[a,*]

[a] *State Key Laboratory for Mechanical Behavior of Materials, Xi'an Jiaotong University, Xi'an 710049, PR China*

[b] *Department of Mechanical Engineering, Materials Science and Engineering Program, Texas A&M University, College Station, TX 77843-3123, USA*

Received 23 December 2011; accepted 26 December 2011
Available online 2 January 2012

The strain hardening behavior of nanolayered Cu/Zr micropillars was studied using the microcompression technique, which revealed that both the strain hardening exponent and the strain hardening rate are controlled by the intrinsic rather than extrinsic size. The maximum strain hardening rate is observed at a layer thickness of ~20 nm, which can be explained physically in terms of reduced dislocation storage rates. A dislocation model is modified to elucidate the dislocation storage in the nanolayered materials and predicts a critical intrinsic size below which the strain hardening rate drops off.

Keywords: Nanolayered micropillar; Strain hardening; Dislocation storage; Size effect

Nanostructured metallic multilayers are used in a variety of applications because of the ease of tailoring the fabrication of these structures to meet specific property needs [1,2], and they provide ideal systems for the exploration of length scale dependent plasticity [3–5]. Generally, the hardness/strength of multilayers (e.g. Cu/Nb [4,5], Cu/Cr [6], Cu/Ni [7], Cu/Ag [8] and Cu/Zr [5]) increases monotonically with decreasing individual layer thickness (h) down to ~1–5 nm, as is consistent with the tenet of "smaller is stronger". In traditional nanoindentation hardness measurements with a sharp indenter tip, the plastic zone has a non-uniform stress state within the sample, thereby making the interpretation of plastic flow behavior complicated and not permitting the observation of strain hardening/softening behavior [9,10]. Microcompression methodology [11] has opened new routes for studying the strain hardening behavior (strain hardening exponent, n, and strain hardening rate, θ) of these nanolaminates at small length scales in a nominally homogeneous stress state [12–14].

Both the strain-hardening exponent (n) and strain hardening rate (θ) are important parameters reflecting a metallic material's hardening property and its determination is of great importance in that it signifies the strain hardening characteristic of a material, which are closely linked to the stored dislocation density [15]. For example, the n value of microcrystal Cu (with high uniform elongation ~20%) is as high as ~0.4–0.5 [16] much higher than that of nanocrystalline Cu (with limited tensile ductility ~2%) <0.2 [17], because in nanocrystalline dislocations emitted from grain boundaries (GBs) can freely run across the grain interior and were absorbed by opposite GBs with little accumulation within grains [18,19].

Recently, Kiener and co-workers [20,21] found that the strain hardening rates of single crystal Cu pillars are strongly dependent on the extrinsic size (pillar diameter). In contrast, Bhattacharyya et al. [14] investigated the intrinsic size (layer thickness, h) effect on the strain hardening rate of Al/TiN multilayers by using a micropillar compress test and found extraordinarily high values of θ in the Al. Misra et al. [22] investigated the work hardening of $h = 30$ nm Cu/Nb multilayers by room temperature rolling and found that the multilayers showed low θ (~300–350 MPa), with lower $n \sim 0.25$ compared with their bulk coarse-grained monolithic constituents. The observed reduced work hardening capacity (low θ) in nanolayered Cu/Nb may be interpreted in terms of glide dislocation interactions with interface

* Corresponding authors. Tel.: +86 (0) 2982668695; fax: +86 (0) 2982663453 (J. Sun); e-mail addresses: lgsammer@mail.xjtu.edu.cn; zhangx@tamu.edu; junsun@mail.xjtu.edu.cn

[1] These authors contribute equally to this paper.

1359-6462/$ - see front matter © 2011 Acta Materialia Inc. Published by Elsevier Ltd. All rights reserved.
doi:10.1016/j.scriptamat.2011.12.032

dislocations, allowing for cross-slip and annihilation-related recovery processes [22]. Detailed analysis is still needed, however, especially in modeling the work hardening rate in nanolayered materials. In this paper, we report the intrinsic (h) rather than extrinsic (ϕ) size-controlled work hardening behavior of nanolayered Cu/Zr micropillars by using a microcompression test and qualitatively and simply interpreted the maximum strain hardening rate in terms of a reduced storage rate of dislocations.

Cu/Zr multilayers, ~1.6 μm thick, with equal h varying from 5 to 100 nm, were deposited on HF-etched Si (100) substrates by direct current magnetron sputtering at room temperature. Then the focused ion beam (FIB) machined micropillars, with ϕ spanning from 300 to 800 nm, fabricated from the multilayers were uniaxially compressed in a Hystron Ti 950 triboindenter with a 10 μm side flat quadrilateral cross-section diamond indenter at a loading rate of ~0.35 nm s^{-1} (corresponding to a constant strain rate of 2×10^{-4} s^{-1}) up to 15–30% strain. Force–displacement data were continuously recorded, and the initial geometry of the pillar was measured from scanning electron microscopy (SEM) images (see Fig. 1). More details on the fabrication of the micropillars and the calculation procedure to determine the true stress–strain curves can be found in our previous work [13].

Figure 1(a)–(f) compares FIB/SEM images taken before and after uniaxial compression of the $\phi = 800$ nm pillars with $h = 100$ nm (a, b), $h = 50$ nm (c, d) and $h = 20$ nm. It can be seen that the deformed $h = 100$ nm pillar shows plastic barreling and extrusion of material from the individual Cu layers. In contrast, the deformed pillars with $h = 20$ nm and below show shear deformation across the compression plane without significant barreling or extrusion. For the intermediate $h = 50$ nm pillar, both barreling (accompanied with extrusion) and shearing are observed. The intrinsic size-dependent transition of the deformation mode is similar to that of compressed Al/Pd micropillars [12], whereas the extrinsic size dependence of the deformation behavior is quite weak. The deformation mechanism of Cu/Zr micropillars transforms from preferential thinning (squeezing out) of Cu at larger h to shear localization at smaller h (<50 nm). This is attributed to the transitioning from dislocation-dominated symmetric slip at large h to shear localization induced by asymmetric slip and grain boundary-mediated deformation at small h [13].

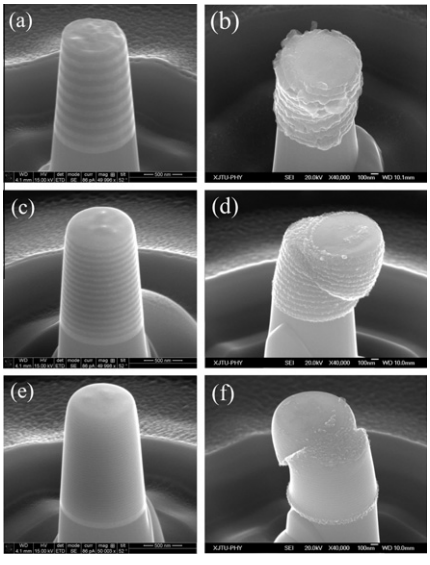

Figure 1. SEM images of the $\phi = 800$ nm Cu/Zr micropillars with three different values of h, before and after the uniaxial compression tests. As-milled micropillar with (a) $h = 100$ nm, (c) $h = 50$ nm and (e) $h = 20$ nm; (b) $h = 100$ nm micropillar after compression showing barreling of the micropillar and extrusion from individual Cu layers; (d) $h = 50$ nm micropillar after compression showing squeezing and shearing of the pillar; and (f) $h = 20$ nm micropillar after compression showing shearing the micropillar.

Representative compressive true stress–strain curves corresponding to the deformation of pillars with $h =$ 10 nm of three different diameters are shown in Figure 2(a), from which several features can be observed: (i) a gradual transition between elastic and plastic deformation; (ii) after the stress reaches a maximum, a gradual softening occurs until failure ensues; and (iii) the strain hardening behavior can be described by Ludwik's equation [13,17], i.e., $\sigma = K_1 + K_2\varepsilon_p^n$, where K_1 represents the initial yield stress, K_2 is the strengthening coefficient and n is the strain hardening exponent. The n values determined for the three extrinsic sized pillars exhibited the same fashion – n monotonically decreasing with reducing h – and are quite close to each other for pillars with the same h (see Fig. 2(a) and (b)), indicating that n is strongly intrinsic size dependent. For example, the values of n for $\phi = 300$ and 800 nm Cu/Zr 10 nm pillars are about 0.3 and 0.325, respectively.

Interestingly, a scaling relationship is revealed for all three ϕ values when the strain hardening exponent n is depicted with respect to the strength σ_{max}, as shown in Figure 2(c). The figure shows a reasonably linear relationship between the measured n values and the σ_{max} strength values: the higher the n, the lower the σ_{max}. This indicates that, under constant ϕ, the hardening exponent

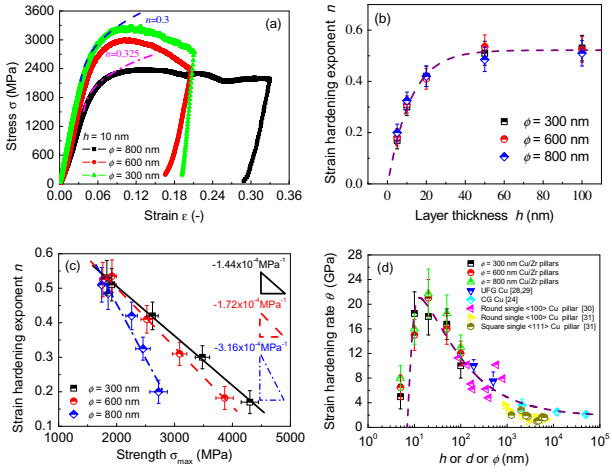

Figure 2. (a) True stress–strain plot for $h = 10$ nm Cu/Zr pillars with varies ϕ. The strain hardening regime (Regime II) is fitted by using Eq. (2). (b) n as a function of h. (c) The n–σ_{max} curves for Cu/Zr pillars with three different values of ϕ. (d) θ fitted by Eq. (8). The θ of microcrystalline Cu [24], ultrafinecrystalline Cu [25,26] and single crystal Cu pillars [20,21] are also plotted for comparison.

n of nanolayered micropillars is inversely proportional to the strength. The Cu/Zr micropillars with $\phi = 800$ nm have a scaling slope of -3.16×10^{-4} MPa^{-1}, a factor $\sim$2 higher than those with $\phi = 300$ nm. This means that increasing the strength by the same amount will cause a greater reduction in the strain hardening exponent n (or hardening capacity) for Cu/Zr micropillars with a larger ϕ.

Additionally, the strain hardening rate θ of Cu/Zr pillars with various diameters was determined by the difference between the strength at 0.2% and 2% plastic strain, which is consistent with the θ values at small plastic strain estimated from these fitting curves (see Fig. 2(d)) by using the strain rate hardening equation, i.e. $\theta = \frac{d\sigma}{d\varepsilon}$.

It is found that in this ϕ scale (300–800 nm) the strain hardening rate θ is independent of ϕ within the scatter, but is strongly dependent on h and is much higher than that of microcrystals, as shown in Figure 2(d). The maximum strain hardening rate θ was observed at a critical layer thickness h^{cri} of $\sim$20 nm. The inverse layer thickness (or grain size d) effect reported here has also been observed in Cu films with thickness range spanning from 20 to 800 nm [23]. Below h^{cri}, the strain hardening rate θ decreases with decreasing h; above h^{cri}, a smaller h leads to a higher θ, similar to coarse ultrafine-grained pure metals (e.g. Cu [24–26]) and single crystal Cu pillars [20,21] with ϕ in the range of 90–8000 nm, as shown in Figure 2(d). As pointed out in our previous work [13], this is because more glide-interface dislocation interactions result in increasing θ with reducing h to a critical value $\sim$20 nm, below which the dislocation cross-slip lowers the θ, thus leading to the inverse dependence of θ on h. Here, we further found that the inverse h effect is independent of extrinsic size at such a length scale. The underlying physical mechanism is the intrinsic size-dependent dislocation storage capacity [15,24,27]. Major advances investigating the crystalline plasticity in the nanometer grains in depth revealed that the accumulation of a high density of dislocations emitted from GB/interface (on the order of $\sim 10^{16}$ m^{-2}) inside nanograins is found to be possible [28] when they are surrounded by neighboring grains, due to image force [29] from the surface that pull the dislocations out of grain is significantly reduced [28].

Based on the SEM observations, one can find that the Cu layers provide the majority of the plastic strain. This implies that the soft Cu layers dominate the strain hardening behavior of Cu/Zr multilayers. According to the strain hardening theory [27], the relation between the stress σ and the dislocation density ρ can be described by the Taylor relationship as,

$$\sigma = \frac{1}{s} kb\mu^* \sqrt{\rho} \tag{1}$$

where s is the Schmid factor, and is $\sim$0.33; κ is a proportionality constant, and is $\sim$0.2–0.5; b is the magnitude of the Burgers vector; $\mu^* = \frac{\mu_{Zr} \cdot \mu_{Cu}}{V_{Zr} \cdot \mu_{Cu} + V_{Cu} \cdot \mu_{Zr}}$ is the effective shear modulus of the Cu/Zr multilayers, which can be estimated by the shear moduli μ_{Cu} and volume fractions V_{Cu} of the Cu and Zr layers. In multilayers, the density of dislocation nucleated from the GB/interface sources [19,31] ρ_{nucl} at a given plastic stain ε_p is $\rho_{nucl} = \varepsilon_p/(bl)$ [30], where l is the average distance of slip of dislocations proportional to h. From an atomistic point of view, the dislocation length L becomes increasingly important as the material's characteristic dimensions (d or h or ϕ) reach the nanoscale. Carlton and Ferreira [32] proposed a model of statistical absorption of dislocations by GBs applicable in nanoscaled materials. Similar to the nanocrystalline GBs, the interfaces of multilayers can also act as dislocation sources and/or sinks [19,31]. Therefore, according to this model [31], the probability of a dislocation being absorbed by the interface, P_{dis}, can be expressed by:

$$P_{dis} = \left\{ 1 - \left[1 - \exp\left(\frac{-(\Delta G + \tau_0 b^3)}{k_B T} \right) \right]^{\frac{sbv}{\dot{\varepsilon} h}} \right\}^{\omega L}, \tag{2}$$

where $p = \exp[-(\Delta G + \tau_0 b^3)/(k_B T)]$ is the probability of an atom successfully jumping into the grain boundary in a single attempt; $N = (sbv)/(\dot{\varepsilon} h)$ is the number of attempted jumps by dislocation core atoms to the GB during a given time; $J = \omega L$ is the total number of atoms on the dislocation core jumping into the GB; ΔG is the heats of mixing-dependent interface energy for activation of atomic migration (or dislocation nucleation) and varies within the range 0.2–2 eV for incoherent interface [31]; $k_B = 1.38 \times 10^{-23}$ J K^{-1} is Boltzmann's constant; T is temperature; L is the dislocation length, and is proportional to the layer thickness h; $\dot{\varepsilon}$ is the strain rate; ν is the Debye frequency; τ_0 is the resolved shear stress; ω physically corresponds to the atomic linear density of the dislocation core and is independent of grain size; and other symbols have the same meaning as above. By using $\Delta G = 0.825$ eV [31], $\tau_0 = s\sigma_0 = 41$ MPa [32], $b = 0.2556$ nm, $T = 300$ K, $\nu = 7.2 \times 10^{12}$ Hz, $L = h$, $\dot{\varepsilon} = 2 \times 10^{-4}$ s^{-1}, $\omega = 2.5$ atoms nm^{-1} and Eq. (2), we found that $P_{dis} = 0$ at $h \geqslant 20$ nm, below which the trapping/absorption of dislocations by GBs and/or interfaces is more prevalent (for $h = 10$ nm, $P_{dis} = 0.076$; for $h = 5$ nm, $P_{dis} = 0.887$). This is probably the underlying reason for the monotonically reduced n.

We further consider that the flow stress and strain hardening rate of a material may be described based on the evolution of a single parameter: the total density of dislocation ρ ($\rho = \rho_{stor} + \rho_{intf} + \rho_{fib}$, where ρ_{stor} is the dislocation density stored within the grain interior, the interfacial dislocation density ρ_{intf} is a function of strain ρ_{fib} is the dislocation density introduced by the FIB machining, and is of the order of $\sim 10^{12}$–10^{14} m^{-2} [33]). To quantitate the effect of the size effect on the strain hardening behavior within a common approach, we use the Kocks–Mecking–Estrin (KME) model of strain hardening [27], following the treatment of Estrin et al. [15]. The net rate of dislocation storage with imposed strain, therefore, can be written as:

$$\frac{d\rho}{d\varepsilon_p} = \frac{1}{b}\frac{dL}{da} = \frac{1}{s}\left[\frac{1}{b\Lambda} - g\rho \right] \tag{3}$$

where dL represents the length of dislocation stored per area swept da, g is the strain rate- and temperature-dependent coefficient ($\sim$20 [15]), which describes the kinetics of dynamic recovery irrespective of the grain size, and Λ may be called a "mean free path" and can be given as [27],

$$\frac{1}{\Lambda} = \frac{1 - P_{\text{dis}}}{h} + \chi\sqrt{\rho} \tag{4}$$

where χ is a parameter, of the order of ~0.0375 [15], which can be expressed in terms of the stage II strain hardening coefficient for a coarse-grained material. This dislocation accumulation rate is a fundamental quantity in the dislocation theory of strain hardening. It is accessible by experimentation: differentiating Eq. (1) gives:

$$\sigma\frac{d\sigma}{d\varepsilon_{\text{p}}} = \frac{1}{2}\left(\frac{kb\mu^*}{s}\right)^2\frac{d\rho}{d\varepsilon_{\text{p}}} \tag{5}$$

With the definition of θ, and inserting Eq. (3) into Eq. (5), one may also write this as:

$$\theta = \frac{k\mu^*}{2s^2\sqrt{\rho_{\text{stor}} + \rho_{\text{intf}} + \rho_{\text{fib}}}}\left[\frac{1}{\Lambda} - gb(\rho_{\text{stor}} + \rho_{\text{intf}} + \rho_{\text{fib}})\right] \tag{6}$$

where

$$\rho_{\text{stor}} = \rho_{\text{nucl}}(1 - P_{\text{dis}}) = \varepsilon_{\text{p}}(1 - P_{dis})/(bl) \tag{7}$$

Assume that $\rho_{\text{fib}} \approx 10^{12}\ \text{m}^{-2}$, therefore, the Eq. (6) can be rewritten as follows:

$$\theta = \frac{k\mu^*}{2s^2}\left[\frac{(1 - P_{\text{dis}})}{h}\sqrt{\frac{bl}{\varepsilon_{\text{p}}(1 - P_{\text{dis}}) + bl(\rho_{\text{intf}} + \rho_{\text{fib}})}} - \sqrt{\frac{\varepsilon_{\text{p}}(1 - P_{\text{dis}}) + bl(\rho_{\text{intf}} + \rho_{\text{fib}})}{bl}} + \chi\right] \tag{8}$$

Here all the symbols have the same meaning as before. The tension data on multilayers showed a low strain hardening rate after the initial 1–2% plastic strain [4]. Taking a series of parameters with $\kappa = 0.25$, $\mu^* = 40.6$ GPa, $b = 0.2556$ nm, $\varepsilon_{\text{p}} = 2\%$, $l = h$ and $\rho_{\text{intf}} = 0.02$ nm^{-2}, and with Eq. (8), we plotted θ as a function of characteristic dimension h or d or ϕ, which appears to agree well with the experimental data even at submicron-microns length scale, as shown by the dash line in Figure 2(d).

In summary, the unique strain hardening behavior of nanolayered Cu/Zr pillars is found to be controlled by their intrinsic size instead of their extrinsic size. There is an inversely linear dependence of the strain hardening exponent on the maximum strength. The length scale related storage of dislocation (density) was shown to account for the intrinsic size-dependent strain hardening exponent and the maximum strain hardening rate.

This work was supported by the National Natural Science Foundation of China (50971097), the 973 Program of China (Grant No. 2010CB631003. X.Z. acknowledges the financial support of the NSF-DMR Metallic Materials and Nanostructures Program, under Grant No. 0644835. Discussions with Prof. P.J. Ferreira (University of Texas at Austin) are greatly appreciated.

[1] M.J. Demkowicz, R.G. Hoagland, J.P. Hirth, Phys. Rev. Lett. 100 (2008) 136102.
[2] G.S. Was, T. Foecke, Thin Solid Film 286 (1996) 1.
[3] M.A. Phillips, B.M. Clemens, W.D. Nix, Acta Mater. 51 (2003) 3171.
[4] A. Misra, J.P. Hirth, R.G. Hoagland, Acta Mater. 53 (2005) 4817.
[5] J.Y. Zhang, X. Zhang, R.H. Wang, S.Y. Lei, P. Zhang, J.J. Niu, G. Liu, G.J. Zhang, J. Sun, Acta Mater. 59 (2011) 7368.
[6] J.Y. Zhang, X. Zhang, G. Liu, G.J. Zhang, J. Sun, Mater. Sci. Eng. A 528 (2011) 2982.
[7] Y. Liu, D. Bufford, H. Wang, C. Sun, X. Zhang, Acta Mater. 59 (2011) 1924.
[8] J. McKeown, A. Misra, H. Kung, R.G. Hoagland, M. Nastasi, Scripta Mater. 46 (2002) 593.
[9] S.M. Han, M.A. Phillips, W.D. Nix, Acta Mater. 57 (2009) 4473.
[10] J.R. Greer, J.T.M. De Hosson, Prog. Mater. Sci. 56 (2011) 654.
[11] M.D. Uchic, D.M. Dimiduk, J.N. Florando, W.D. Nix, Science 305 (2004) 986.
[12] P. Dayal, M.Z. Quadir, C. Kong, N. Savvides, M. Hoffman, Thin Solid Film 519 (2011) 3213.
[13] J.Y. Zhang, S.Y. Lei, Y. Liu, J.J. Niu, Y. Chen, G. Liu, X. Zhang, J. Sun, Acta Mater. 60 (2012) 1610.
[14] D. Bhattacharyya, N.A. Mara, P. Dickerson, R.G. Hoagland, A. Misra, Acta Mater. 59 (2011) 3804.
[15] O. Bouaziz, Y. Estrin, Y. Bréchet, J.D. Embury, Scripta Mater. 63 (2010) 477.
[16] M.M. Chaudhri, Acta Mater. 46 (1998) 3047.
[17] L. Lu, X. Chen, X. Huang, K. Lu, Science 323 (2009) 607.
[18] J.Y. Zhang, G. Liu, R.H. Wang, J. Li, J. Sun, E. Ma, Phys. Rev. B 81 (2010) 172104.
[19] M. Dao, L. Lu, R.J. Asaro, J.T.M. De Hosson, E. Ma, Acta Mater. 55 (2007) 4041.
[20] D. Kiener, A.M. Minor, Acta Mater. 59 (2011) 1328.
[21] D. Kiener, P.J. Guruprasad, S.M. Keralavarma, G. Dehm, A.A. Benzerga, Acta Mater. 59 (2011) 3825.
[22] A. Misra, X. Zhang, D. Hammon, R.G. Hoagland, Acta Mater. 53 (2005) 221.
[23] P.A. Gruber, J. Böhm, F. Onuseit, A. Wanner, R. Spolenak, E. Arzt, Acta Mater. 56 (2008) 2318.
[24] C.W. Sinclair, W.J. Poole, Y. Bréchet, Scripta Mater. 55 (2006) 739.
[25] L. Lu, R. Schwaiger, Z.W. Shan, M. Dao, K. Lu, S. Suresh, Acta Mater. 53 (2005) 2169.
[26] E. Ma, Y.M. Wang, Q.H. Lu, M.L. Sui, L. Lu, K. Lu, Appl. Phys. Lett. 85 (2004) 4932.
[27] U.F. Kocks, H. Mecking, Prog. Mater. Sci. 48 (2003) 171.
[28] L. Wang, Z. Zhang, E. Ma, X.D. Han, Appl. Phys. Lett. 98 (2011) 051905.
[29] A. Hartmaier, M.C. Fivel, G.R. Canova, P. Grumbsch, Model. Simul. Mater. Sci. Eng. 7 (1999) 781.
[30] J.C.M. Li, Y.T. Chou, Metal. Mater. Trans. B 1 (1970) 1145.
[31] R.F. Zhang, J. Wang, I.J. Beyerlein, T.C. Germann, Scripta Mater. 65 (2011) 1022.
[32] C.E. Carlton, P.J. Ferreira, Acta Mater. 55 (2007) 3749.
[33] A.T. Jennings, J. Li, J.R. Greer, Acta Mater. 59 (2011) 5627.